MANUSCRIPT UNDER REVIEW (April 2026)

Manuscript title: Extremely fast juvenile growth explains observed unimodal fish length distributions

Authors: Freddie J. Heather[1*], Ken H. Andersen[2], Nils C. Krueck[1], Asta Audzijonyte[1,3]

***Corresponding author**: freddie.heather@utas.edu.au

Affiliations:

1. Institute for Marine and Antarctic Studies, University of Tasmania, Hobart, Australia
2. Natl. Inst. of Aquatic Resources, Technical University of Denmark, Bygning 202, Kgs. Lyngby, Denmark
3. Centre for Marine Socioecology, University of Tasmania, Hobart, Australia

Author contributions: FJH, KHA and AA conceived the study. FJH, KHA, NCK and AA provided critical contributions to the data analysis, development of the first draft and the final version of the manuscript.

Data availability statement: All R code to run the analysis and produce the figures, including data files, can be found at https://github.com/FreddieJH/theory_obs

Data sources: Otolith biochronology data and von Bertalanffy parameters were obtained from published literature. The sources of these are stated in the manuscript. Underwater visual census data were taken from the publicly available Reef Life Survey dataset.

Conflict of interest statement: The authors declare no conflicts of interest.

Acknowledgments: The authors would like to thank E. Trip for providing daily and annual otolith increment data. FJH would also like to thank colleagues at DTU Aqua for ideas in the initial stages of the study, and to DTU Aqua for hosting during this period.

Funding Declaration: This study was supported by the Australian Research Council Discovery Project (DP220102446) to A.A., N.C.K and K.H.A, and a Pew Fellowship in Marine Conservation to A.A.

Abstract

1. Body length distributions for coastal fish have been observed to be unimodal, with the highest abundances at intermediate body sizes and relatively fewer small and large individuals. This empirical pattern contrasts with predictions from widely applied models based on the von Bertalanffy growth function (VBGF), which predict that the smallest individuals are most abundant and that abundance monotonically declines with increasing body length.
2. We investigated whether unimodal body length distributions can arise from realistic growth and mortality dynamics, without assuming VBGF. Using a simple population equilibrium model applied to a suitable case-study species, *Ctenochaetus striatus*, we examined how growth-at-size and mortality-at-size interact to shape the observed body length distributions. Results were evaluated using independent otolith-derived growth rates, including daily-resolution otolith growth increments for the first year of life.
3. When observed body length distributions were used to infer growth-at-size rates across a broad range of plausible mortality scenarios, estimated growth was considerably faster during early ontogeny than predicted by the VBGF. These estimated growth-at-size rates closely matched the independent otolith-derived growth trajectories.
4. Alternatively, when otolith-derived growth rates were incorporated into our population model, the emergent length distributions under a range of plausible mortality-at-size scenarios were all unimodal in shape, resembling empirical observations.
5. Our findings demonstrate that unimodal body length distributions, reported earlier across hundreds of coastal fish species, are not only the consequence of observation selectivity but emerge naturally when rapid early growth is accounted for. These findings also support previous concerns that VBGF strongly underestimates juvenile fish growth.

6. Fish population and community models relying on VBGF-based growth are likely to overestimate the relative abundance of the smallest individuals, potentially biasing inferences about juvenile mortality, predator-prey interactions, and competition. Incorporating realistic growth dynamics will improve the accuracy of population assessments and ecological models, including those used to fisheries management and conservation actions.

Keywords: von Bertalanffy growth, biphasic growth, otolith biochronology, empirical body length, length-frequency, growth-at-size, mortality-at-size

Introduction

The relative abundance of small, medium and large individuals within natural populations is determined by a combination of individual growth, mortality and recruitment (Peters, 1986; Schmidt-Nielsen, 1984). Recruitment is defined as the number of the youngest individuals entering the population in any given year, which drives the overall abundance of the population, and is often assumed to occur at a continuous rate or fluctuating around a constant level (Andersen, 2019). Growth rates determine how quickly individuals grow from smaller to larger length classes, and mortality rates define the loss of individuals from each length class. Thus, the relative rates of mortality and growth (or M/k ratio, Hordyk et al., 2015b) determine the shape of the population body length distribution, with relatively faster growth resulting in a relatively greater abundance of larger individuals and vice versa. The mortality to growth ratio, and resultant body length distribution, is considered a fundamental indicator of a species' ecological role, extinction risk, productivity and resilience (Blueweiss et al., 1978; Olden et al., 2007; Peters, 1986). However, it is unclear how much variation exists in the shape of body length distributions in natural populations (Froese et al., 2018; Hordyk et al., 2015b; Jensen, 1996; Prince et al., 2023). A recent continental-scale analysis of empirically observed body length distributions from visual census datasets covering ~800 diverse rocky and coral reef fish species showed that, for the large majority of populations and species, spatially and temporally pooled length distributions can be approximated by a positive-normal or lognormal statistical distribution (Heather et al., 2025). That is – observed body length distributions were mostly unimodal, with the greatest abundance of individuals occurring at an intermediate body length. This finding contrasts with traditional fisheries models, which typically predict highest abundances in the smallest size groups, unless the mortality to growth ratio is very low (Hordyk et al., 2015a).

The discrepancy in the theoretically expected (monotonically declining) versus observed (unimodal) shapes of body length distributions can be explained in two ways. The first and most intuitive explanation is that selectivity reduces the observed abundance of the smallest

individuals. This could be either through observational selectivity, where the smallest individuals are less likely to be observed or sampled, or ecological selectivity, where the smallest individuals are indeed absent from the surveyed area. However, according to Heather et al. (2025), the selectivity required to reconcile the discrepancy between theory and observations across nearly 800 fish species was considerable. For example, according to classic growth modelling (von Bertalanffy, 1957), and assuming a generic M/k (mortality to growth coefficient) ratio of 1.5 (Froese et al. 2018) and logistic observational selectivity, only about 50% of individuals at 40% of a population's maximum length (L_{max}) would be observed in a population body length distribution sample. In other words, for a species growing to 100 cm in length, only half of 40 cm individuals would be observable compared to observation probability of fully observable sized fish. Such a high level of selectivity needed to explain naturally observed body length distributions seems unrealistically high and not in line with published analysis on size-dependence of observational selectivity in underwater surveys (Ackerman and Bellwood, 2000).

The alternative explanation for higher-than-expected relative numbers of intermediate sized individuals in observed population body length distribution samples is fast growth during early ontogeny. Classic fisheries science typically assumes fish growth following a von Bertalanffy growth function (VBGF), with its growth coefficient (k) representing the instantaneous rate of increase in body length towards the asymptotic body length (L_{∞}). Importantly, the VBGF assumes linearly declining growth rate with body length (Gulland and Holt, 1959), reaching zero growth at the asymptotic body length, L_{∞}. The VBGF k is estimated as a single parameter by fitting the VBGF to individual or population level length-at-age data. However, it is widely acknowledged that VBGF performs poorly in predicting juvenile growth (Day and Taylor, 1997; Lester et al., 2004), leading to over 20 different alternative biphasic growth models suggested to better account for different growth between juvenile and adult individuals (Wilson et al., 2018). Biphasic models typically represent pre-maturation growth as linear, followed by the VBGF or another uniphasic non-linear growth

function after maturation. The key consideration here is that the relative growth of juvenile fish is fast up until around maturation size, from which point on growth declines. Thus, if true growth rates of the smallest individuals are indeed considerably faster than assumed by the VBGF, then the relative numbers of the smallest individuals in an equilibrium population would have to be lower than expected in population models that use VBGF to represent growth. This is because the smallest individuals would quickly grow into intermediate sizes and accumulate there as growth slows down. This process could lead to the observed unimodal, rather than monotonically declining, body length distributions (Heather et al. (2025).

Resolving fundamental uncertainties about the shape (monotonically declining or unimodal) of natural fish populations is important from both a theoretical and practical point of view. While biphasic growth models are increasingly used to better represent individual growth and energy allocation processes (Wilson et al., 2018), VBGF is still the main model used to generate predictions about natural body length distributions in many marine ecological modelling and fisheries applications (e.g., Froese et al., 2018; Hordyk et al., 2015b). However, if classic uniphasic growth models, such as the VBGF, predict unrealistically high relative abundance of juvenile fish in natural populations, there are direct implications for associated inferences of density dependence, species interactions, and other ecological processes. From a fisheries perspective, size-based population models typically assume growth according to the VBGF and that the left side of observed body length distributions is shaped by adequately estimated sampling selectivity (e.g., Froese et al., 2018; Hordyk et al., 2015b). Yet, if growth is biphasic and the true observable body length distribution is unimodal, the estimation of these selectivity parameters will be biased, with important implications for the assessment and management of target species worldwide. Here, we aim to reconcile empirical observations of unimodal body length distributions with theoretically expected monotonically declining distributions by testing whether the apparent lack of the smallest individuals in body length distributions could result from faster than expected

juvenile growth, rather than observational selectivity alone. To achieve this, we use a unique case study and a simple size-based equilibrium model to (1) estimate size-specific growth rates required to match observed unimodal body length distributions and then (2) contrast these inferred growth estimates to independent empirical growth rates derived from otolith analyses.

Methods

Data and species selection

Body length data for wild fish populations were obtained from underwater visual surveys around the Australian continent available from the Reef Life Survey (RLS) program (Edgar et al., 2020; Edgar and Stuart-Smith, 2014). Visual census survey methodology and assessments of its potential biases are described in detail in many previous studies (Edgar et al., 2004; Reef Life Survey Foundation, 2019). Briefly, the surveys are performed according to a standardised protocol, where two divers survey 5 x 50 m transects, counting all observed fish by species and estimating their individual lengths to the nearest body length class, with the width of the length classes increasing as fish get larger (2.5, 5, 7.5, 10, 15, 20, 25… cm).

For this study we selected a case study fish population based the following criteria: 1) no fishing pressure; 2) a common species with many individuals observed in RLS data; 3) enough length classes in observation data to accurately represent the population body length distribution; and 4) the availability of high resolution (daily and annual growth increment) otolith size-at-age data to determine size-specific growth rates across the full species size range. Meeting all these criteria, we selected the lined bristletooth (*Ctenochaetus striatus*) from Mermaid Reef Marine Park, about 280km off the northwest coast of Western Australia. This species is highly abundant in the marine park (n = 8367 total observations), spanning seven body length classes, and had otolith-derived growth rate estimates publicly available (Trip et al., 2014). The Mermaid Reef Marine Park met all the

criteria to be determined as highly effective (no take, well enforced, old, large, and isolated; Edgar et al., 2014) and it included 72 RLS surveys at 18 distinct sites, conducted during 2013 and 2018.

Estimating growth-at-size using empirically observed length distributions

In the first part of analysis, we calculated the growth rates required to produce empirically body length distributions of *C. striatus*, i.e., the temporally and spatially pooled distribution from all the 18 sites and two years of RLS observations (Figure 1). Following methods described in Andersen (2019), we modelled the equilibrium (stable) number of individuals within a body length class as a function of the individuals growing into the length class from the previous (i.e., smaller) length class, which is equal to the individuals growing out into the next (bigger) length class plus the individuals dying from the length class:

$$\mathrm{j}_{i-1}N_{i-1} \;=\; j_i N_i + \mu_\mathrm{i}\, N_i \qquad 1$$

Here $\mathrm{N_i}$ is the number of individuals within length class i, j_i is the rate of growth out of the length class i (units of 'per time') and μ_i is the instantaneous mortality rate for length class i (units of 'per time', also commonly referred to as M).

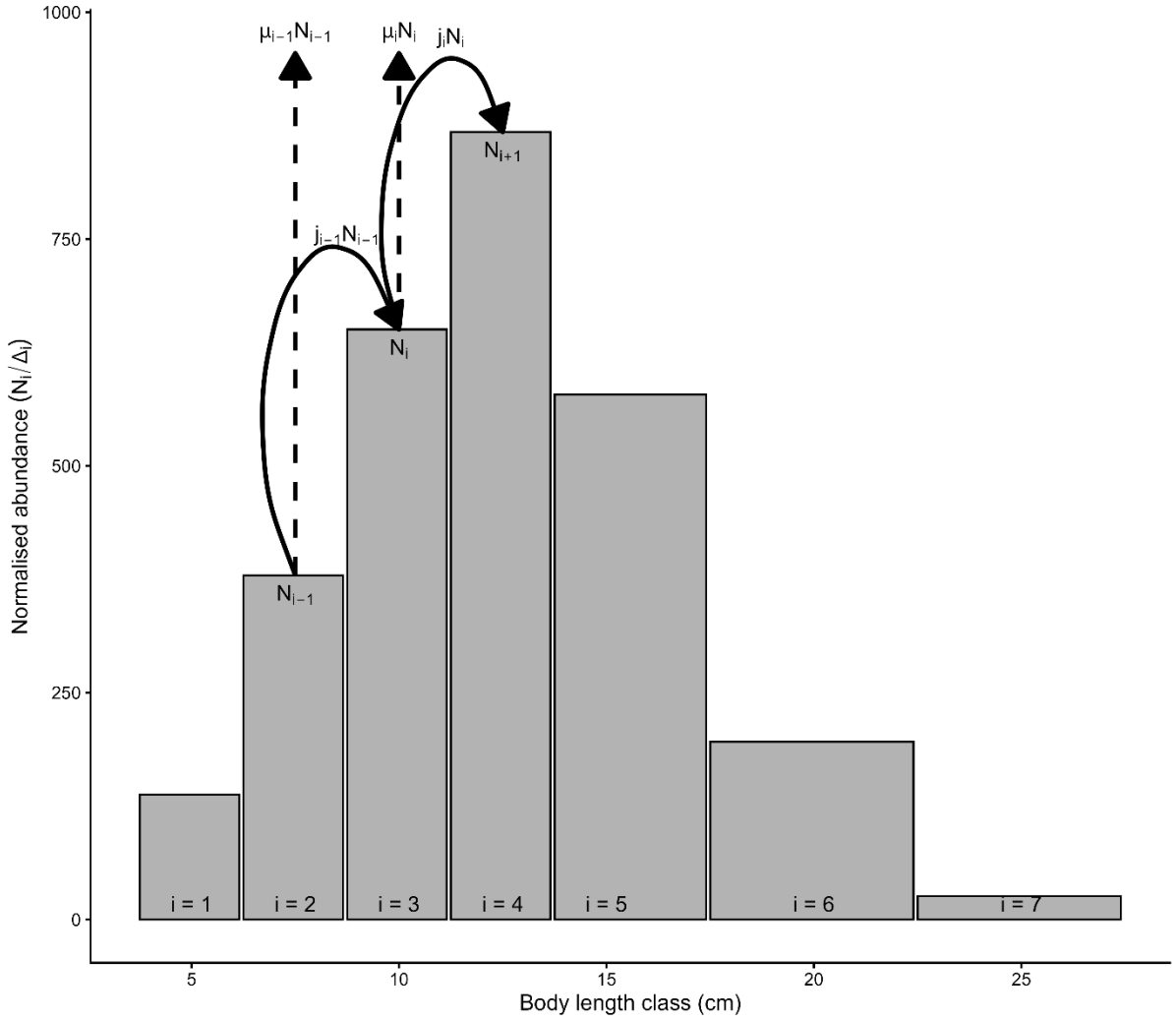

188

189 **Figure 1.** Observed body length distribution for *Ctenochaetus striatus*, with overlayed model
190 concept. The equilibrium abundance, N, within a length class, i, is defined as the number
191 growing into the length class from the previous length class ($j_{i-1}N_{i-1}$), minus the death from
192 the length class (μ_iN_i), minus the number growing out of the length class into the following
193 length class (j_iN_i). See Equation 1. Y-axis represents the normalised abundance (abundance
194 per unit length, where Δ_i is the width of the length class in cm).

195

196 Because the abundance within each of the length classes ($N_1, N_2, N_3, \ldots, N_n$) is known (from
197 the observed survey data), we can assume alternative rates of mortality in each length class
198 (μ_i) to then estimate the associated fraction of individuals growing-in and growing-out (j_{i-1}
199 and j_i) individuals required to produce empirically observed length distributions. For this, we

define the growth rate (g, cm per year) as the fraction of individuals growing out of the length class, j_i, multiplied by the width of the length class, (Δ_i in cm), i.e., $g_i = j_i \Delta_i$. Likewise, we normalise abundances in each length class, by dividing them by length class width, Δ_i to obtain normalised abundance $\mathcal{N}_i$, or the abundance per unit body length. Now we can rearrange and substitute g_i and $\mathcal{N}_i$ into Equation 1 to estimate the growth rate in a previous length class ($i - 1$), given the growth rate in the current length class (i), assuming some mortality in the length class (see supplementary material S1 for derivation):

$$g_{i-1} = \frac{\mathcal{N}_i}{\mathcal{N}_{i-1}} (g_i + \mu_i \Delta_i) \quad 2$$

If we assume that the growth rate in the largest length class is zero, we can work backwards to estimate the growth rate within each previous length class that would give rise to the observed length distribution, since $\mathcal{N}_i / \mathcal{N}_{i-1}$ is known (observed). Alternatively, the same results can be obtained by re-arranging Equation 2 to estimate the growth rate in the following class ($i + 1$ class) as a function of the growth in the current class i. However, the latter option requires assuming some growth rate at the smallest length class, which is more uncertain than assuming the final growth rate to be zero. We therefore used the former option and calculate growth backwards through the size classes (as shown in Equation 2).

Since we do not know the true natural mortality-at-size (μ_i), we started by testing three different mortality-at-size assumptions - constant, linearly declining and exponentially declining (Lorenzen et al., 2022). According to Lorenzen et al. (2022), natural mortality across sizes can be represented by a scaling exponent of approximately -1, i.e., $M = aL^{-1}$ or in our case $\mu_i = a{L_i}^{-1}$, where a is a scaling constant representing 'mortality-at-unit-length', with a median value of 16.3 at 1 cm body length. Here we compare the exponentially declining *M* ($\mu_i = 16.3{L_i}^{-1}$) to constant *M* at size ($\mu_i = b$) and to linearly declining mortality ($\mu_i = c + dL_i$). Values of parameters b, c, and d, were selected so that the total mortality ($\sum_{i=1} \mu_i$) in the three scenarios was the same (see supplementary material S2).

We also explored how changes in Lorenzen's mortality exponent, scaling coefficient (mortality-at-unit-length), and assumptions about senescence mortality, μ_s, might affect growth rate estimates. For this we first tested ten different exponent values for natural mortality, ranging from -0.81 to -1.02 (Lorenzen, 2022), equally spaced. To explore the effect of the scaling coefficient, we tested three values – the median value reported by Lorenzen et al. (2022) of 16.3/year at 1 cm length, and a lower and upper bounds covering one order of magnitude, or 5 to 50 (units of per year, at 1 cm body length). To model senescence mortality, μ_s we used a function that increases hyperbolically as it approaches the maximum observed length class: $\mu_{s,i} = s/(\max(L) - L_i + 1\ \mathrm{cm})$, with three values of the constant s representing no senescence (s = 0 cm/year), medium senescence mortality rate (s = 0.5 cm/year), and high senescence mortality (s = 1 cm/year). Two sensitivity analyses were performed. First, each of the ten Lorenzen mortality exponents (where the mortality scaling coefficient was fixed at 16.3) were combined with the three levels of senescence mortality assumptions to explore impacts on estimated growth rates, totalling 30 mortality scenarios. Secondly, each of the three Lorenzen mortality scaling coefficient (where the mortality exponent was fixed at -1) were combined with the three levels of senescence mortality assumptions, totalling nine mortality scenarios.

For each calculated growth-at-size values from the scenarios above the resulting individual size-at-age curves were plotted for the estimated maximum age of 36 years (Choat and Robertson, 2002). For this the growth-at-size rate was linearly interpolated between the body length classes using the *interp1* function from the *pracma* package (Borchers, 2023), and this growth-at-size rate was then numerically solved using the *ode* function from the *deSolve* package (Soetaert et al., 2010) to obtain the size-at-age from zero to 36 years.

Validating growth-at-size estimates

In the following, we compared the growth rates that were required to produce the observed length distribution of *Ctenochaetus striatus* (estimated as described above, using 39

mortality scenarios) with (1) population level growth rate estimates obtained from published VBGF parameters and (2) independent growth rates from otolith biochronologies of the same species. According to VBGF, the growth-at-size (g) (note, it is different from the more usually used growth-at-age) decreases linearly with increasing body size (L), becoming zero at asymptotic length (L_∞) (Gulland and Holt, 1959):

$$g = \frac{\mathrm{d}L}{\mathrm{d}t} = k(L_\infty - L) \quad (3)$$

Seven estimates of the VBGF parameters for unfished *C. striatus* populations from the Indo-Pacific region were available from Trip et al. (2008) (Table 1) and were used to estimate and plot growth-at-size (Figure 3).

Table 1. von Bertalanffy growth function parameter estimates for *Ctenochaetus striatus* from unfished locations (Fishing Pressure = "None" in Trip et al., 2008) around the Indo Pacific region, taken from Trip et al. (2008).

L_∞ (cm)	k	t0	Size-range (FL, cm)	N	Ocean	Population
17.1	0.9	-0.4	13.3-20.2	80	W. S. Pacific	Lizard Island (outer)
18.8	0.4	-0.6	8.4-25.2	40	Indian	Cocos Keeling lagoon
19.4	1.0	-0.3	8.6-23.0	117	W. S. Pacific	Lizard Island
19.4	0.4	-0.7	12.3-21.0	35	Indian	Cocos Keeling
19.9	0.3	-0.8	15.0-23.3	116	W. S. Pacific	One Tree Island
20.1	0.8	-0.3	12.1-28.8	85	W. S. Pacific	Townsville
23.2	1.3	-0.2	17.9-25.9	45	Indian	Oman

Next, growth-at-size was calculated from high resolution individual level otolith size-at-age biochronologies, combining growth increments at both the daily and annual resolution (Trip et al., 2014). This level of resolution was required to accurately represent growth rates in

youngest and smallest individuals, especially important to determine growth in individuals prior to the formation of the first annual increment. The biochronology data was available for 415 individuals (319 at the annual resolution and 96 at the daily resolution; Trip et al., 2014) and these data were used to estimate an average growth-at-age, by fitting a regression model to the size-at-age data. We first fit a log-linear function to 415 individual-level the body size-at-age:

$$L = \beta_0 + \beta_1 \ln(A) \quad (4)$$

where A is age in years, differentiating with respect to age gives the instantaneous growth rate, g:

$$g = \frac{\mathrm{d}L}{\mathrm{d}t} = \beta_1 / e^{(L-\beta_0)/\beta_1} \quad (5)$$

For direct comparison of the body length between the otolith-derived growth rate and observed surveyed body length data, length should be represented as total length (TL). Of the 415 individuals with biochronology data, TL was available for 238 (58%), however fork length (FL) was available for all 415. We therefore fitted a simple linear allometric model to estimate TL from FL ($\mathrm{TL} = \beta_2 + \beta_3 \mathrm{FL}$) from the 238 individuals where both TL and FL were reported (Figure S3.3). See supplementary material S3 for the model fitting procedure of the size-at-age (Equation 4) and allometric model (Equation 5).

Calculating the length distribution from individual growth rates

Finally, we conducted an alternative test and asked – what kind of body length distribution would emerge from empirical otolith-derived growth rates? In contrast to the analyses above, where we used length distribution as a basis to calculate required growth rate, here we are using growth rates as a basis to calculate the emergent length distribution. In this analysis we use otolith-derived growth-at-size as described above to calculate the body length distribution that would emerge from such growth, under some mortality assumption. This is done by rearranging Equation 2 to estimate the abundance within each length class as a

function of the abundance of the previous length class, otolith-derived growth rates (Trip et al., 2014) and alternative rates of mortality-at-size:

$$\mathcal{N}_i = g_{i-1}(g_i + \mu_i \Delta_i)\mathcal{N}_{i-1} \quad (6)$$

For mortality-at-size (μ_i) we used all 39 mortality scenarios defined above.

Results

Growth-at-size required to produce observed length distributions

Given the observed unimodal body length distribution (Figure 2D), under nine mortality scenarios with three different scaling coefficient values for the Lorenzen's exponential mortality curve (all with an exponent of -1) and three levels of senescence mortality (Figure 2C), the estimated growth-at-size followed an approximate exponential decline, i.e., approximately linear on the log-scale (Figure 2A). Varying the scaling coefficient (from 5 to 50/year) also varied the intercept (on the log-scale) of the estimated growth-at-size (Figure 2A), with the estimated growth-at-size values at smallest sizes (5 cm) ranging from approximately 25 to 250 cm/year. Changing the exponent of the mortality-at-size (from -0.81 to -1.02), but keeping the scaling coefficient fixed at the medial value of 16.3/year, only had a minor effect on the shape of the estimated growth-at-size and size-at-age curves (supplementary material S4). In all cases (either with varying exponent or scaling coefficient), including senescence mortality led to slightly higher estimated growth rates and suggested growth acceleration in larger length classes (Figure 2A); the acceleration of growth in large individuals was higher for higher senescence mortality rates. This overall higher growth rate and especially the growth acceleration at larger sizes meant that when senescence mortality was included the estimated size-at-age curves approached asymptotic sizes faster (most opaque lines in Figure 2B).

Assuming constant or linearly declining mortality-at-size versus Lorenzen's exponential mortality did not have a large effect on the calculated growth-at-size, when the overall mortality remained equal. That is, across all mortality scenarios, estimated growth rates

declined exponentially with increasing body sizes (further details in supplementary material S2).

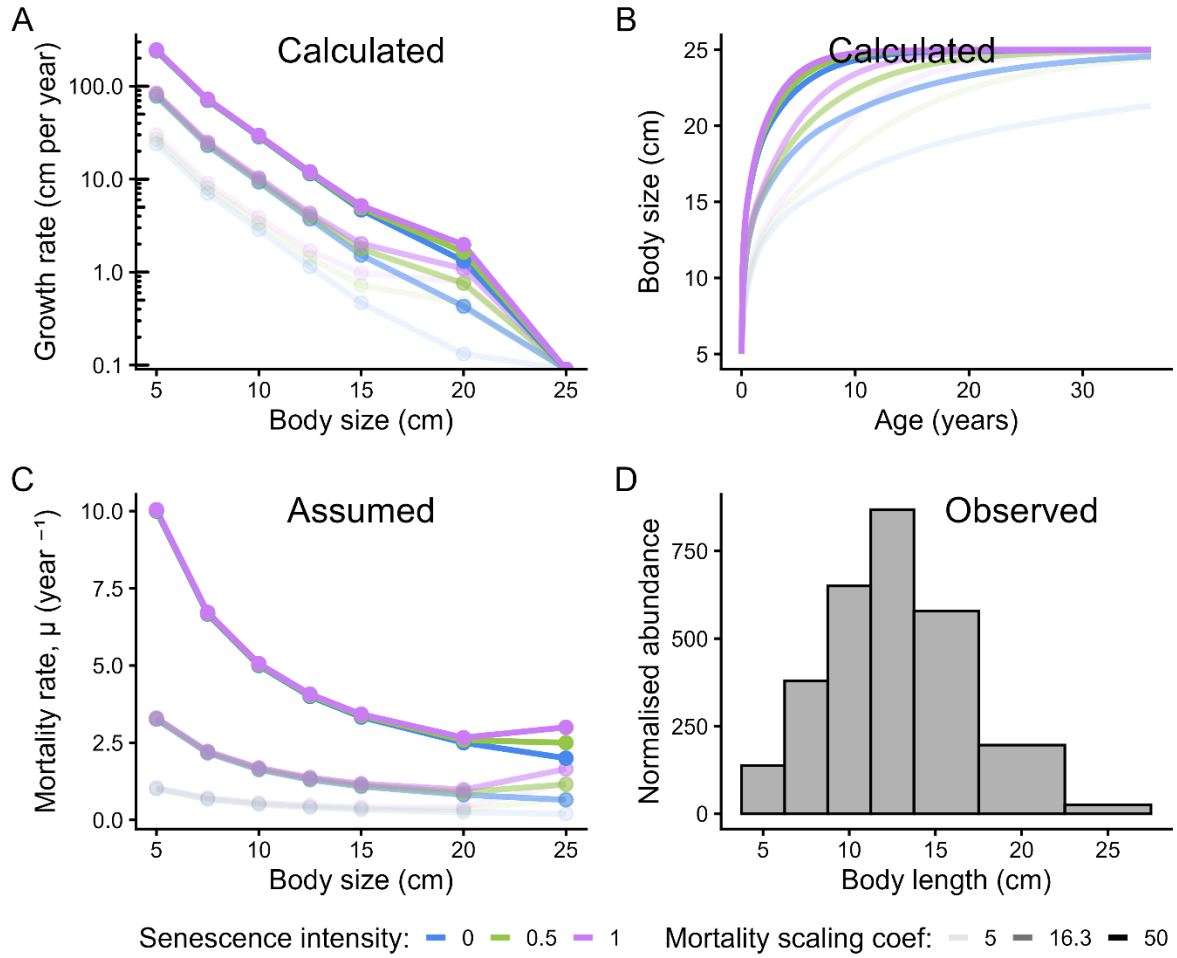

Figure 2. Estimated growth-at-size (A) and size-at-age (B) for various plausible Lorenzen mortality scenarios (C) that would result in the observed (D) length distribution of *Ctenochaetus striatus*. Mortality scenarios include three different mortality scaling coefficients (line transparency), each combined with three levels of senescence mortality (line colours).

Comparing estimated growth rates with VBGF estimates and otolith data

Our analyses showed that the growth-at-size required to reproduce the observed length distribution declined with body length exponentially (Figure 2A, Figure 3). Importantly, a similar exponential decline was also seen in the growth rate derived from the empirical

otolith size-at-age data for this species (solid black line in Figure 3; Trip et al., 2014). In contrast, the linear decline in growth-at-size assumed by VBGF function and resulting from population-level parameter estimates (dashed black lines in Figure 3, n = 7 parameter sets presented in Table 1) generally gave considerably lower growth-at-size rates at smallest body lengths.

The results from otolith growth data confirmed exponentially declining growth-at-size (Figure 3), with growth rates at 5 cm length 92.9 cm/year (76 to 118, 95% confidence intervals) and then declining to an average of 0.06 cm/year (0.05 to 0.07, 95% confidence intervals) for the largest individuals at 25 cm. The regression model (Equation 4) fitted to otolith biochronology data gave β_0 and β_1 parameter estimates as 14.6 (standard error = 0.13, $p < 0.001$) and 2.72 (standard error = 0.066, $p < 0.001$), respectively (see supplementary material S3 for model checks and model summary statistics).

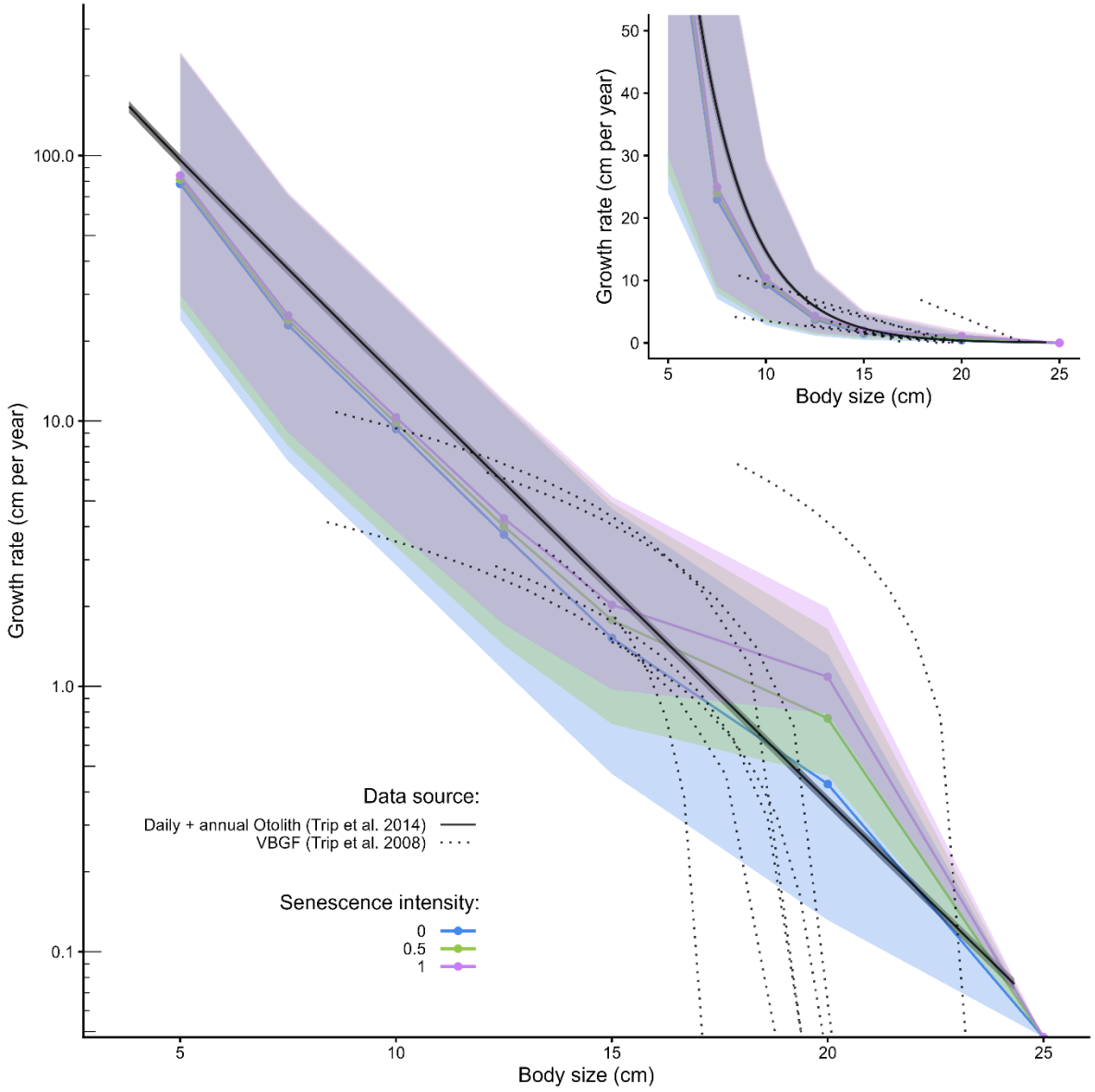

342

343 **Figure 3**. Comparison of growth-at-size estimates for *Ctenochaetus striatus* based on the
344 observed length distribution and assumed Lorenzen mortality scenarios (coloured lines),
345 estimated from VBGF parameters (dashed black lines; Trip et al., 2008) and derived from
346 otolith size-at-age (black solid line; Trip et al., 2014). Ribbons around the estimated growth-
347 at-size represent the plausible range of mortality-at-unit-length (mortality scaling coefficient)
348 values described by Lorenzen et al. (2022). Inset shows the same plot but on the linear
349 rather than logarithmic y scale (y axis cropped for clarity).

350

Length distributions obtained from empirically observed individual growth rates

In the final part of analysis, we asked whether unimodal body size distributions would emerge from empirically observed (otolith-derived) growth rates (reported in the previous section). Given the otolith-derived growth rates for each size class (Equation 5), and assuming nine scenarios of exponential mortality with varying scaling coefficients and different senescence mortality (Figure 4B), the emergent body length distribution was unimodal in all cases. When median mortality scaling coefficient was used ($\mu_i = 16.3{L_i}^{-1}$, units of per year) (Lorenzen et al., 2022), the peak abundance was observed at 12.5 cm length class, which corresponded with the peak abundance size class in the visual survey data (solid lines in Figure 4C). The lowest mortality scaling coefficient (5/year, i.e., $\mu_i = 5{L_i}^{-1}$), which represented lowest likely values of absolute mortality rate, resulted in more left-skewed emergent body length distribution with relatively lower number of smaller bodied individuals and peak abundance at 12.5 cm, 15 cm or 20 cm length class for the no, medium or high levels of senescence mortality, respectively. (dotted line in Figure 4B). On the other hand, a high scaling coefficient (50/year, i.e., $\mu_i = 50{L_i}^{-1}$) resulted in relatively larger numbers of smallest fish and peak abundance in the 10 cm size class (dashed line in Figure 4B). Scenarios with different mortality exponents (using the median scaling coefficient of 16.3) had relatively minor impacts on emergent length distribution (supplementary material S4).

Under the median mortality scenario and intermediate senescence assumption, the emergent abundance in the smallest reported length class (5 cm) was similar to the observed (1.04x), while the lowest and highest mortality scaling coefficient scenarios resulted in relatively (0.47x) and higher (2.64x) expected numbers compared to those observed in the field. The relative expected abundance in the largest length class (25 cm) was lower than observed in the field observations under the median mortality scenario (0.51x, under intermediate senescence). When the mortality scaling coefficient was low, the expected numbers in the largest size bins were larger than observed (2.69x), whereas if the

mortality scaling coefficient was very high, the expected numbers were much lower than observed (0.03x). Senescence mortality had a minor effect on the overall unimodal shape of the emergent body length distribution but resulted in a slight decrease in the relative abundances in the larger body length classes, and slight increase in the smaller body length classes (Figure 4). This senescence mortality impact was more pronounced in the lower mortality scenario (dotted lines in Figure 4), than the higher mortality scenario (dashed lines in Figure 4).

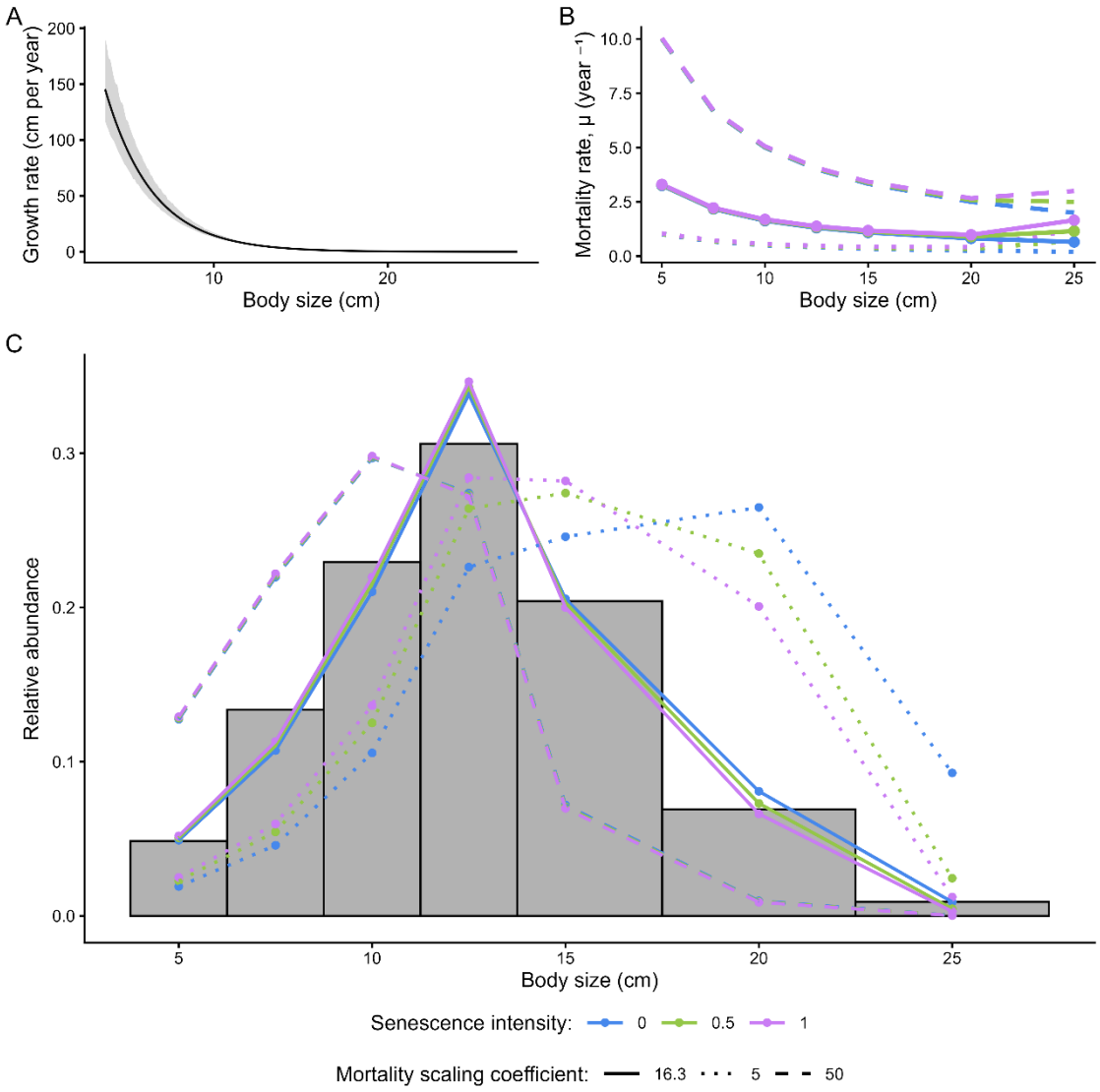

Figure 4. Growth rates and mortality assumptions used to estimate the emergent body length distribution of *Ctenochaetus striatus*. (A) - the empirical otolith growth-at-size, (B) - nine assumed mortality scenarios, (C) - the emergent body length distributions (lines) compared to those observed distribution in visual surveys (grey bars). Relative normalised abundances in C are scaled so that the total numbers in each case sum to one.

Discussion

Knowledge of the expected relative abundance of the smallest, intermediate and largest individuals in a population, and how these abundances are shaped by underlying ecological and physiological processes, is of fundamental importance to population ecology (Peters, 1986). Much of the research on body size-abundance relationships in ecology has focused on the community-level (White et al., 2007), where a population is the fundamental unit defined by some body size metric, such as the average body size, and related to the average density (Damuth, 1987). Theoretical foundations for expected body size distributions within populations have received broader attention only relatively recently and have been advanced largely in the context of fish population dynamics research for management applications (Froese et al., 2018; Hordyk et al., 2015a, 2015b; Prince et al., 2015, 2023).

Our work has important implications for models based on fish population dynamics, such as the length-based spawning potential ratio (LBSPR) population assessment framework by Hordyk et al. (2015a, 2015b), and the application of size spectrum theory by Andersen (2019). Hordyk et al. (2015a) explored body length distribution shapes in equilibrium populations under different mortality to growth (M/k) ratios, assuming that growth follows the VBGF form as fitted to length-at-age data for various species. In contrast, the Andersen (2019) framework is entirely size-structured and similar to the one used in our study, except that it includes reproductive allocation at size and applies general allometric rules to

calculate size-specific mortality and growth. Importantly, both approaches fundamentally assume that individual growth follows the VBGF and that populations are in equilibrium with continuous recruitment. Thus, under most empirically supported growth and mortality parameterisations (Hordyk et al., 2015a, 2015b; Prince et al., 2023), both frameworks expect largest numbers of fish in smallest size class, unless the M/k ratio is very low (e.g., M/k < 0.6; Hordyk et al., 2015a; Prince et al., 2015).

Evaluating how well VBGF-informed theoretical predictions describe natural populations is challenging, primarily because the smallest individuals are rarely sampled effectively in standard surveys (Sheaves et al., 2020). The discrepancy between the left-hand side (small-bodied individuals) of predicted versus observed body length distributions is therefore almost universally attributed to sampling and is used to estimate sampling selectivity parameters (Froese et al., 2018; Hordyk et al., 2015; Rudd & Thorson, 2018). Some degree of selectivity against small individuals is undoubtedly present in nearly all sampling methods but estimating selectivity from body length distributions requires assumption about the true underlying population length distribution, and this is generally assumed to be monotonically declining. Recent work challenges this assumption, since across nearly 3000 populations of coral and rocky reef fishes, empirically observed length distributions were overwhelmingly unimodal (Heather et al., 2025). The key question then becomes whether this unimodal shape is entirely an artefact of selectivity, or whether natural population body length distributions are indeed unimodal. In other words, does the peak abundance of individuals in an average population (pooled over time and space) indeed occur at some intermediate body size? Analyses presented in this study suggest that the answer to this question might be positive and point to a biologically well-supported driver – growth of the smallest individuals is considerably faster than assumed by the widely used VBGF.

Fast juvenile growth explains unimodal length distributions

The notion that VBGF underestimates juvenile growth is not new (e.g., Gamito, 1998). The extensive development of biphasic growth models (Quince et al., 2008a, 2008b) reflects a

long-standing recognition that juvenile growth is often rapid and distinctly slowing down at around maturation size (e.g., Day and Taylor, 1997; Lester et al., 2004; Wilson et al., 2018). Alternatives to VBGF, such as the Gompertz (Gompertz, 1825), Schnute-Richards (Schnute and Richards, 1990), the generalised VBGF (Pauly, 1979), logistic, and power-law (Rafail, 1971) functions, often outperform VBGF but with no clear dominant model (Katsanevakis, 2006; Katsanevakis and Maravelias, 2008; Zhang et al., 2020). This fast growth at smaller size is also supported by experimental studies (e.g., Jobling, 1983) and otolith-based growth reconstructions (e.g., Morrongiello and Thresher, 2015), which consistently demonstrate very fast early growth and a sharp decline as fish grow to larger sizes. Under such growth dynamics, the emergence of a unimodal equilibrium length distribution is a natural outcome – individuals pass quickly through small size classes and accumulate at intermediate sizes where growth slows, analogous to the formation of traffic jams where vehicle speed is reduced. Importantly, our simulations show that empirically derived otolith growth rates under reasonable mortality scenarios are sufficient to generate unimodal length distributions that closely resemble those observed in underwater visual surveys.

Our findings highlight that von Bertalanffy growth trajectories (linearly declining growth-at-size) differ substantially in shape from otolith-derived growth trajectories (exponentially declining growth-at-size) or from growth rates required to produce observed time- and space-pooled body length distributions (exponentially declining growth-at-size). Our results corroborate concerns about the poor fitting of VBGF to smaller bodied individuals within natural populations and highlight that this misfit has direct consequences for predicting population length distributions, including potential downstream applications in support of fishery assessment and management (Froese et al., 2018; Hordyk et al., 2015b).

Clearly, visual census and nearly any other fish sampling method has some selectivity, but estimating selectivity parameters based on the assumption of monotonically declining length frequencies could also be misleading. Visual census methods likely underrepresent the smallest-bodied individuals due to their cryptic behaviour (Ackerman & Bellwood, 2000;

Willis, 2001) and may also misrepresent larger bodied individuals due to a tendency to overestimate body sizes (Edgar et al., 2004), or because larger, faster swimming individuals may avoid divers or enter the survey area after the transect has begun, introducing sampling bias in non-instantaneous counts (Ward-Paige et al., 2010). Surprisingly, when median absolute mortality rate was used, we observed effectively no difference in the observed and expected estimated abundance of the smallest bodied individuals (5 cm length class), but if absolute mortality is higher, then some underestimation in smallest size groups is likely. Future studies should explore more empirically derived growth rates and emergent length distributions across a broader range of species, but it is essential that they use daily or at least weekly estimates of growth in youngest fish, because annual growth increments don't provide sufficient resolution to reconstruct growths in early ontogeny.

Implications of von Bertalanffy growth function use in population and fisheries models

Our comparison of growth models highlights a discrepancy between von Bertalanffy growth trajectories and empirically derived or inferred growth-at-size relationships. Exponential decline in growth-at-size, as shown here, is much more compatible with the biphasic growth framework, which is theoretically well developed (Quince et al., 2008a, 2008b; Wilson et al., 2018). However, the VBGF is deeply rooted in fisheries science models, which are primarily concerned with adult components of populations (the depletion of reproducing individuals), and is unlikely to be abandoned in the near future given its mathematical simplicity, convenience, and extensive historical use. Our findings do not imply that models based on von Bertalanffy growth should be abandoned, specifically not where growth is described well by the VBGF or in cases where management objectives focus on adult individuals. However, since reference points inferred from various established stock assessment approaches are rooted in fish population dynamic theory based on the VBGF, we do highlight the need for caution when these approaches are used to predict and interpret population-level size distributions, estimate selectivity (Beverton and Holt, 1959, 1957), or infer ecological processes involving juvenile stages. If natural populations have fewer small individuals (or

juveniles) than predicted by the VBGF, these models may incorrectly assume that more small fish exist but are simply not observed. Such systematic underestimation of juvenile growth and overestimation of their relative abundances may have implications for population and community models that make inferences about predator-prey interactions, competition or early mortality rates. Importantly, systematically misrepresenting selectivity may also lead to systematic bias in population depletion estimates, with important potential implications for sustainable fisheries management.

References

Ackerman, J., Bellwood, D., 2000. Reef fish assemblages: a re-evaluation using enclosed rotenone stations. Mar. Ecol. Prog. Ser. 206, 227–237. https://doi.org/10.3354/meps206227

Andersen, K.H., 2019. Fish ecology, evolution, and exploitation: a new theoretical synthesis. Princeton University Press.

Beverton, R., Holt, S., 1959. A review of the lifespans and mortality rates of fish in nature, and their relation to growth and other physiological characteristics. Wiley Online Library.

Beverton, R., Holt, S., 1957. On the dynamics of exploited fish populations. Her Majesty's Stationary Office.

Blueweiss, L., Fox, H., Kudzma, V., Nakashima, D., Peters, R., Sams, S., 1978. Relationships between body size and some life history parameters. Oecologia 37, 257–272. https://doi.org/10.1007/bf00344996

Borchers, H.W., 2023. pracma: Practical Numerical Math Functions. https://doi.org/10.32614/CRAN.package.pracma

Choat, J.H., Robertson, D.R., 2002. Age-Based Studies, in: Coral Reef Fishes. Elsevier, pp. 57–80. https://doi.org/10.1016/B978-012615185-5/50005-0

Damuth, J., 1987. Interspecific allometry of population density in mammals and other animals: the independence of body mass and population energy-use. Biological

Journal of the Linnean Society 31, 193–246. https://doi.org/10.1111/j.1095-8312.1987.tb01990.x

Day, T., Taylor, P.D., 1997. Von Bertalanffy's Growth Equation Should Not Be Used to Model Age and Size at Maturity. The American Naturalist 149, 381–393. https://doi.org/10.1086/285995

Edgar, G.J., Barrett, N.S., Morton, A.J., 2004. Biases associated with the use of underwater visual census techniques to quantify the density and size-structure of fish populations. Journal of Experimental Marine Biology and Ecology 308, 269–290. https://doi.org/10.1016/j.jembe.2004.03.004

Edgar, G.J., Cooper, A., Baker, S.C., Barker, W., Barrett, N.S., Becerro, M.A., Bates, A.E., Brock, D., Ceccarelli, D.M., Clausius, E., Davey, M., Davis, T.R., Day, P.B., Green, A., Griffiths, S.R., Hicks, J., Hinojosa, I.A., Jones, B.K., Kininmonth, S., Larkin, M.F., Lazzari, N., Lefcheck, J.S., Ling, S.D., Mooney, P., Oh, E., Pérez-Matus, A., Pocklington, J.B., Riera, R., Sanabria-Fernandez, J.A., Seroussi, Y., Shaw, I., Shields, D., Shields, J., Smith, M., Soler, G.A., Stuart-Smith, J., Turnbull, J., Stuart-Smith, R.D., 2020. Establishing the ecological basis for conservation of shallow marine life using Reef Life Survey. Biological Conservation 252, 108855. https://doi.org/10.1016/j.biocon.2020.108855

Edgar, G.J., Stuart-Smith, R.D., 2014. Systematic global assessment of reef fish communities by the Reef Life Survey program. Sci Data 1, 140007. https://doi.org/10.1038/sdata.2014.7

Edgar, G.J., Stuart-Smith, R.D., Willis, T.J., Kininmonth, S., Baker, S.C., Banks, S., Barrett, N.S., Becerro, M.A., Bernard, A.T.F., Berkhout, J., Buxton, C.D., Campbell, S.J., Cooper, A.T., Davey, M., Edgar, S.C., Försterra, G., Galván, D.E., Irigoyen, A.J., Kushner, D.J., Moura, R., Parnell, P.E., Shears, N.T., Soler, G., Strain, E.M.A., Thomson, R.J., 2014. Global conservation outcomes depend on marine protected areas with five key features. Nature 506, 216–220. https://doi.org/10.1038/nature13022

Froese, R., Winker, H., Coro, G., Demirel, N., Tsikliras, A.C., Dimarchopoulou, D., Scarcella, G., Probst, W.N., Dureuil, M., Pauly, D., 2018. A new approach for estimating stock status from length frequency data. ICES Journal of Marine Science 75, 2004–2015. https://doi.org/10.1093/icesjms/fsy078

Gamito, S., 1998. Growth models and their use in ecological modelling: an application to a fish population. Ecological Modelling 113, 83–94. https://doi.org/10.1016/S0304-3800(98)00136-7

Gompertz, B., 1825. On the nature of the function expressive of the law of human mortality, and on a new mode of determining the value of life contingencies. Philosophical transactions of the Royal Society of London 513–583.

Gulland, J.A., Holt, S.J., 1959. Estimation of Growth Parameters for Data at Unequal Time Intervals. ICES Journal of Marine Science 25, 47–49. https://doi.org/10.1093/icesjms/25.1.47

Heather, F., Richards, S., Krueck, N., Stuart-Smith, R., Brandl, S., Casey, J., Edgar, G., Barrett, N., Parravicini, V., Audzijonyte, A., 2025. Consistent Unimodal Body Length Distributions in Hundreds of Reef Fishes Across Diverse Life Histories. Fish and Fisheries 26, 533–545.

Hordyk, A., Ono, K., Sainsbury, K., Loneragan, N., Prince, J., 2015a. Some explorations of the life history ratios to describe length composition, spawning-per-recruit, and the spawning potential ratio. ICES Journal of Marine Science 72, 204–216. https://doi.org/10.1093/icesjms/fst235

Hordyk, A., Ono, K., Valencia, S., Loneragan, N., Prince, J., 2015b. A novel length-based empirical estimation method of spawning potential ratio (SPR), and tests of its performance, for small-scale, data-poor fisheries. ICES Journal of Marine Science 72, 217–231. https://doi.org/10.1093/icesjms/fsu004

Jensen, A.L., 1996. Beverton and Holt life history invariants result from optimal trade-off of reproduction and survival.

Jobling, M., 1983. Growth studies with fish—overcoming the problems of size variation. Journal of Fish Biology 22, 153–157. https://doi.org/10.1111/j.1095-8649.1983.tb04735.x

Katsanevakis, S., 2006. Modelling fish growth: Model selection, multi-model inference and model selection uncertainty. Fisheries Research 81, 229–235. https://doi.org/10.1016/j.fishres.2006.07.002

Katsanevakis, S., Maravelias, C.D., 2008. Modelling fish growth: multi-model inference as a better alternative to a priori using von Bertalanffy equation: Modelling fish growth. Fish and Fisheries 9, 178–187. https://doi.org/10.1111/j.1467-2979.2008.00279.x

Lester, N.P., Shuter, B.J., Abrams, P.A., 2004. Interpreting the von Bertalanffy model of somatic growth in fishes: the cost of reproduction. Proc. R. Soc. Lond. B 271, 1625–1631. https://doi.org/10.1098/rspb.2004.2778

Lorenzen, K., 2022. Size- and age-dependent natural mortality in fish populations: Biology, models, implications, and a generalized length-inverse mortality paradigm. Fisheries Research 255, 106454. https://doi.org/10.1016/j.fishres.2022.106454

Lorenzen, K., Camp, E.V., Garlock, T.M., 2022. Natural mortality and body size in fish populations. Fisheries Research 252, 106327. https://doi.org/10.1016/j.fishres.2022.106327

Morrongiello, J.R., Thresher, R.E., 2015. A statistical framework to explore ontogenetic growth variation among individuals and populations: a marine fish example. Ecological Monographs 85, 93–115. https://doi.org/10.1890/13-2355.1

Olden, J.D., Hogan, Z.S., Zanden, M.J.V., 2007. Small fish, big fish, red fish, blue fish: size-biased extinction risk of the world's freshwater and marine fishes. Global Ecol Biogeography 16, 694–701. https://doi.org/10.1111/j.1466-8238.2007.00337.x

Pauly, D., 1979. Gill size and temperature as governing factors in fish growth: A generalization of von Bertalanffy's growth formula. Berichte des Institut fur Meereskunde an der Universitat Kiel 63, 156.

Peters, R.H., 1986. The ecological implications of body size. Cambridge university press.

Prince, J., Hordyk, A., Valencia, S.R., Loneragan, N., Sainsbury, K., 2015. Revisiting the concept of Beverton-–-Holt life-history invariants with the aim of informing data-poor fisheries assessment. ICES Journal of Marine Science 72, 194–203. https://doi.org/10.1093/icesjms/fsu011

Prince, J.D., Wilcox, C., Hall, N., 2023. How to estimate life history ratios to simplify data-poor fisheries assessment. ICES Journal of Marine Science 80, 2619–2629. https://doi.org/10.1093/icesjms/fsad026

Rafail, S.Z., 1971. A new growth model for fishes and the estimation of optimum age of fish populations. Mar. Biol. 10, 13–21. https://doi.org/10.1007/BF02026761

Reef Life Survey Foundation, 2019. Standardised Survey Procedures for Monitoring Rocky & Coral Reef Ecological Communities. [WWW Document]. URL https://reeflifesurvey.com/wp-content/uploads/2019/02/ NEW-Methods-Manual_150815.pdf

Schmidt-Nielsen, K., 1984. Scaling: why is animal size so important? Cambridge university press.

Schnute, J.T., Richards, L.J., 1990. A unified approach to the analysis of fish growth, maturity, and survivorship data. Canadian Journal of Fisheries and Aquatic Sciences 47, 24–40.

Sheaves, M., Bradley, M., Herrera, C., Mattone, C., Lennard, C., Sheaves, J., Konovalov, D.A., 2020. Optimizing video sampling for juvenile fish surveys: Using deep learning and evaluation of assumptions to produce critical fisheries parameters. Fish and Fisheries 21, 1259–1276. https://doi.org/10.1111/faf.12501

Soetaert, K., Petzoldt, T., Setzer, R.W., 2010. Solving Differential Equations in R: Package deSolve. Journal of Statistical Software 33, 1–25. https://doi.org/10.18637/jss.v033.i09

Trip, E., Choat, J., Wilson, D., Robertson, D., 2008. Inter-oceanic analysis of demographic variation in a widely distributed Indo-Pacific coral reef fish. Mar. Ecol. Prog. Ser. 373, 97–109. https://doi.org/10.3354/meps07755

Trip, E.D.L., Craig, P., Green, A., Choat, J.H., 2014. Recruitment dynamics and first year growth of the coral reef surgeonfish Ctenochaetus striatus, with implications for acanthurid growth models. Coral Reefs 33, 879–889. https://doi.org/10.1007/s00338-014-1182-x

von Bertalanffy, L., 1957. Quantitative laws in metabolism and growth. The quarterly review of biology 32, 217–231.

White, E.P., Ernest, S.K.M., Kerkhoff, A.J., Enquist, B.J., 2007. Relationships between body size and abundance in ecology. Trends in Ecology & Evolution 22, 323–330. https://doi.org/10.1016/j.tree.2007.03.007

Wilson, K.L., Honsey, A.E., Moe, B., Venturelli, P., 2018. Growing the biphasic framework: Techniques and recommendations for fitting emerging growth models. Methods Ecol Evol 9, 822–833. https://doi.org/10.1111/2041-210X.12931

Zhang, K., Zhang, J., Li, J., Liao, B., 2020. Model selection for fish growth patterns based on a Bayesian approach: A case study of five freshwater fish species. Aquat. Living Resour. 33, 17. https://doi.org/10.1051/alr/2020019

S1. Rearranging Equation 1 to estimate growth-at-size

Equation 1 in the main text states that the abundance within a size bin at equilibrium can be defined as the abundance in the previous bin (N_{i-1}) multiplied by the proportion of those growing out of the size bin (j_{i-1}), minus the numbers growing out ($j_i N_i$) and the numbers dying ($\mu_\mathrm{i}\, N_i$):

$$\mathrm{j}_{i-1} N_{i-1} \;=\; j_i N_i + \mu_\mathrm{i}\, N_i \qquad S1.1$$

We can define the growth rate (g, cm per year) as the fraction of individuals growing out of the size bin, j_i, multiplied by the width of the size bin, (Δ_i in cm), i.e., $g_i = j_i \Delta_i$. We can also define the normalised abundance ($\mathcal{N}_i$) as the abundance in the size bin (N_i) divided by the bin width: $\mathcal{N}_i = N_i / \Delta_i$. Substituting these values the $\mathcal{N}$ and g, we get:

$$\left(\frac{g_{i-1}}{\Delta_{i-1}}\right)\left(\mathcal{N}_{i-1}\Delta_{i-1}\right) \;=\; \left(\frac{g_i}{\Delta_i}\right)\left(\mathcal{N}_i\Delta_i\right) + \mu_\mathrm{i}\,\left(\mathcal{N}_i\Delta_i\right) \qquad \mathrm{S1.2}$$

Which simplifies to:

$$g_{i-1}\mathcal{N}_{i-1} \;= g_i\mathcal{N}_i + \mu_\mathrm{i}\,\left(\mathcal{N}_i\Delta_i\right) \qquad \mathrm{S1.3}$$

And rearranges to Equation 2 in the main text:

$$g_{i-1} = \left(g_i + \mu_\mathrm{i}\,\Delta_i\right)\left(\frac{\mathcal{N}_i}{\mathcal{N}_{i-1}}\right) \qquad \mathrm{S1.4}$$

S2. Three differing mortality scenarios and the estimation of growth

We tested three contrasting mortality-at-size scenarios, 1) constant, 2) linear declining, and 3) Lorenzen exponential mortality with an exponent of – 1 (i.e., $\mu_i \propto L_i^{-1}$). Constant and linear declining mortality were scaled so that the total mortality ($\sum \mu_i$) is equal between the three scenarios.

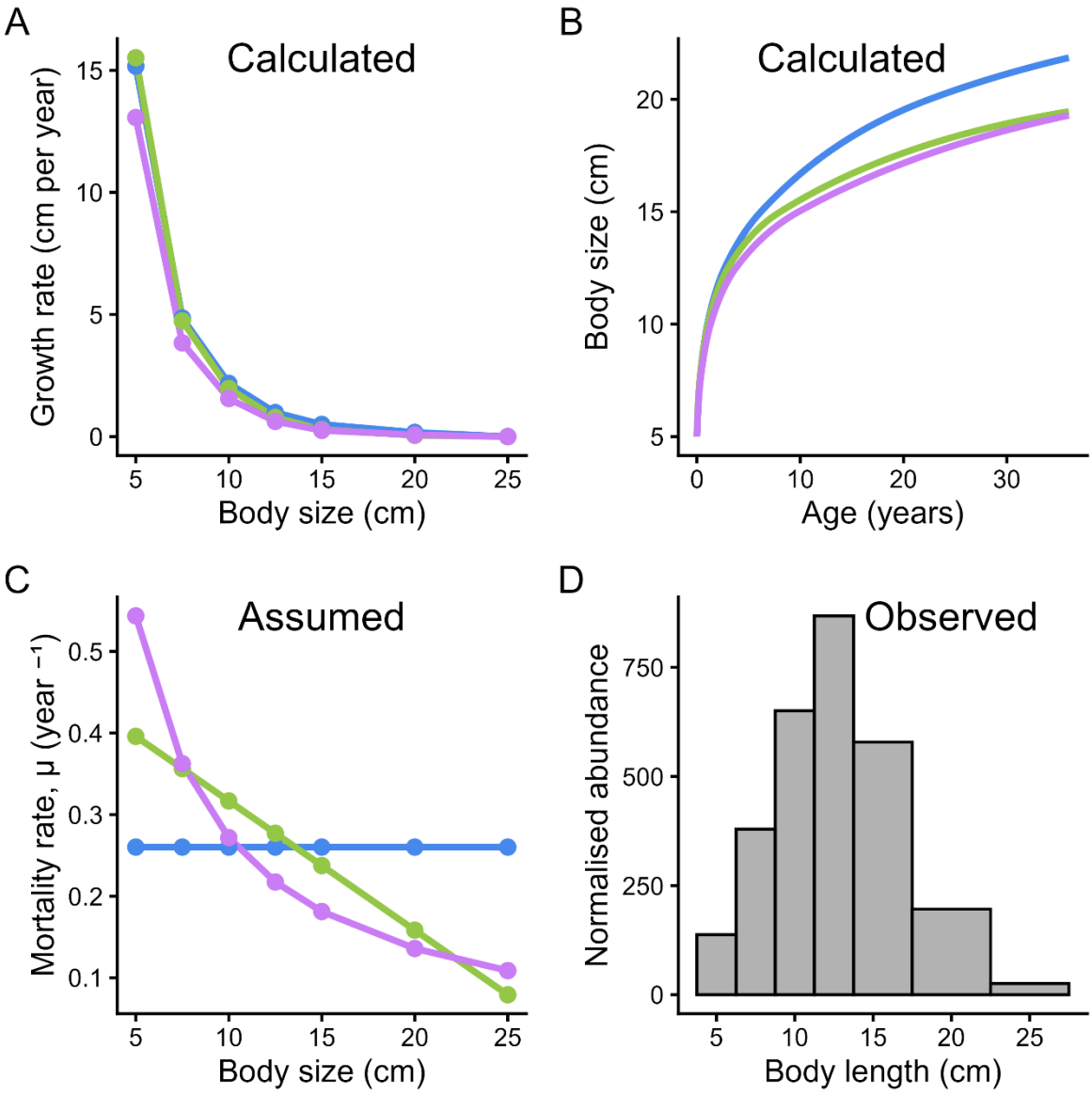

Figure S2.1. Estimated growth-at-size (A) and size-at-age (B) for three mortality scenarios (C) that would result in the observed (D) length distribution of *Ctenochaetus striatus*.

S3. Checking assumptions of otolith statistical model

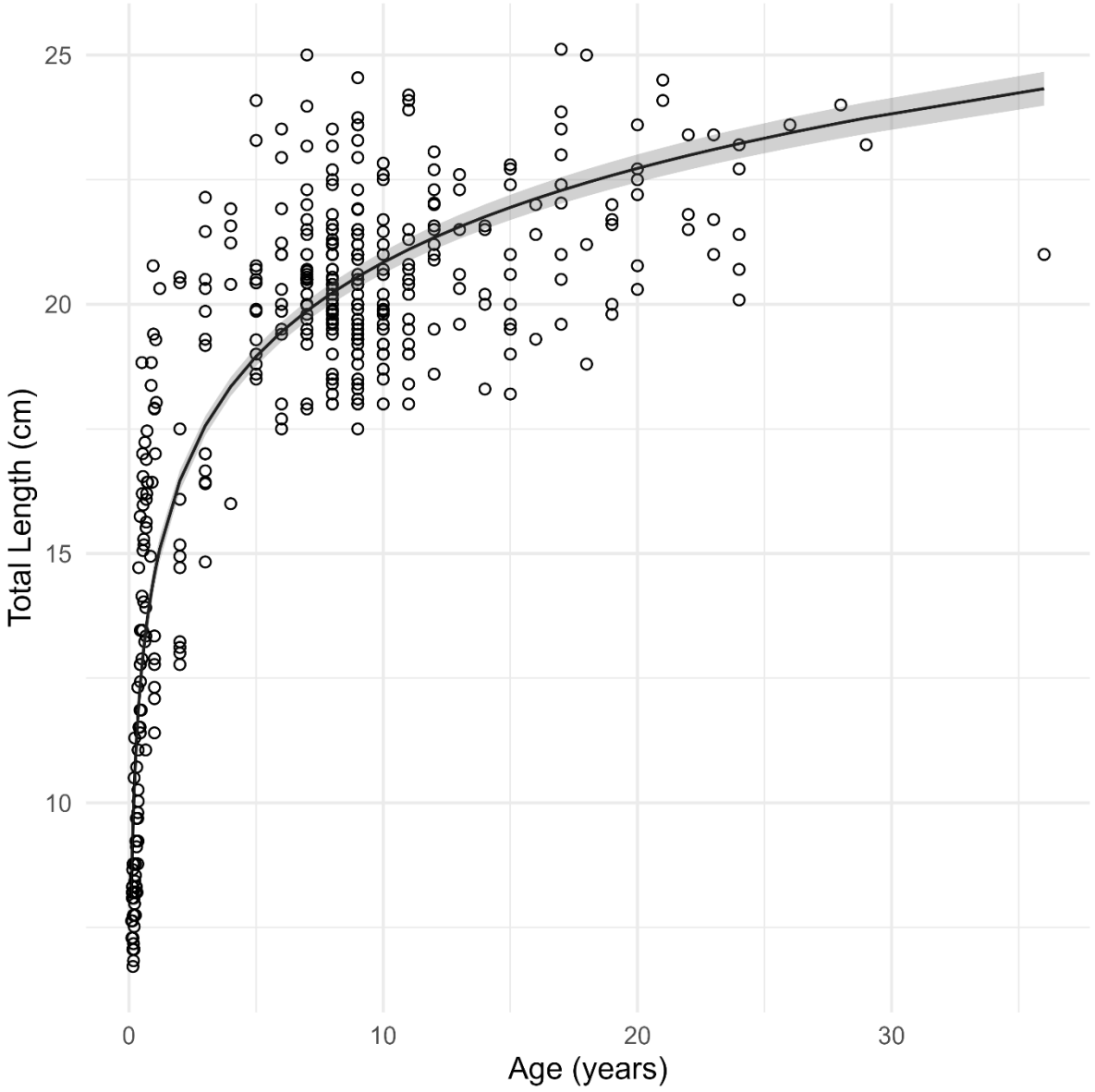

Figure S3.1. Log-linear model fitted to size-at-age for *Ctenochaetus striatus*, using combination of daily and annual otolith growth increments from Trip et al. (2014). Fitted model is: TL = 14.6 + 2.721*log(years).

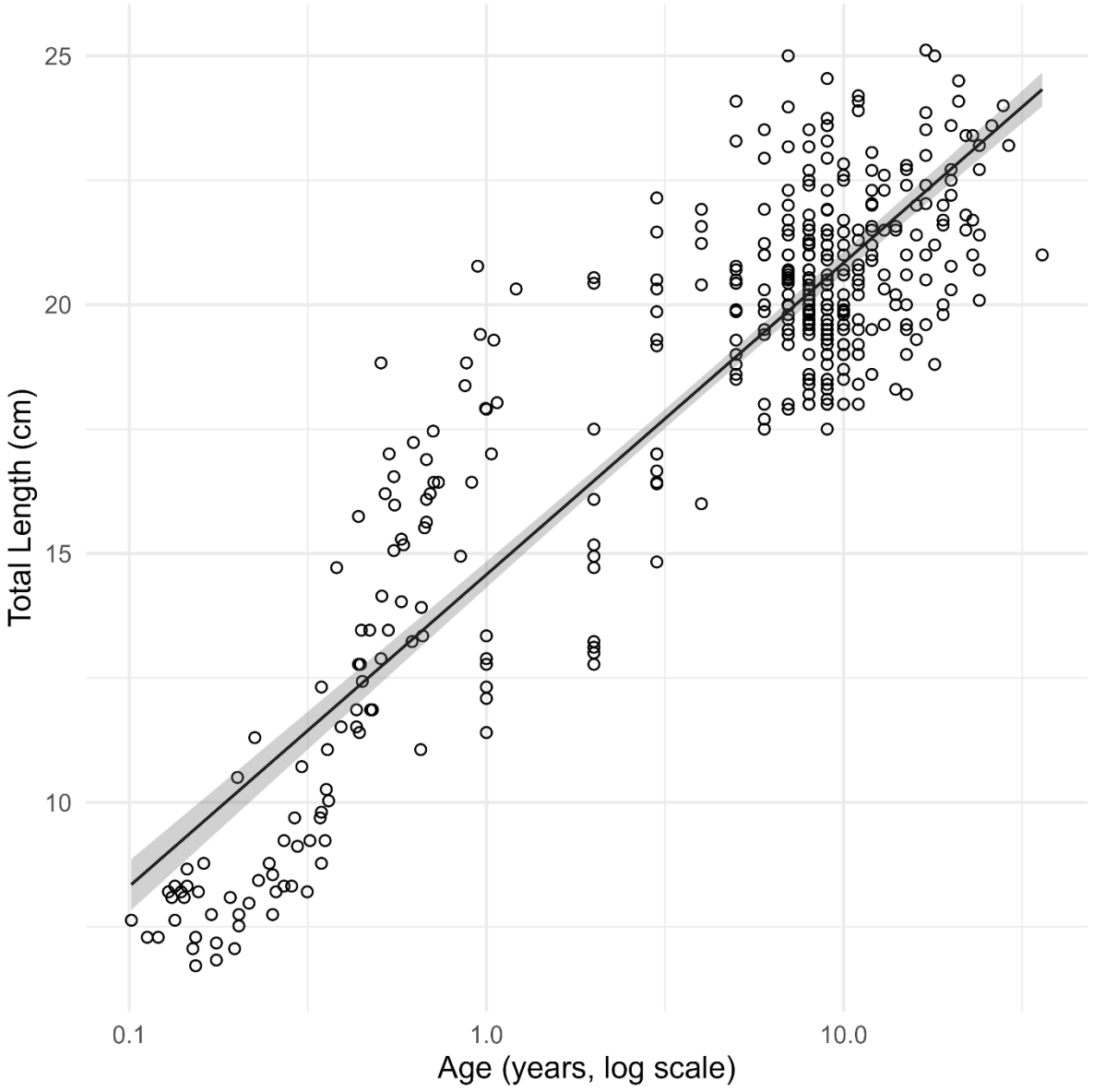

681

682 **Figure S3.2.** Log-linear model fitted to size-at-log(age) for *Ctenochaetus striatus*, using
683 combination of daily and annual otolith growth increments from Trip et al. (2014). Fitted model
684 is: TL = 14.6 + 2.721*log(years).

685

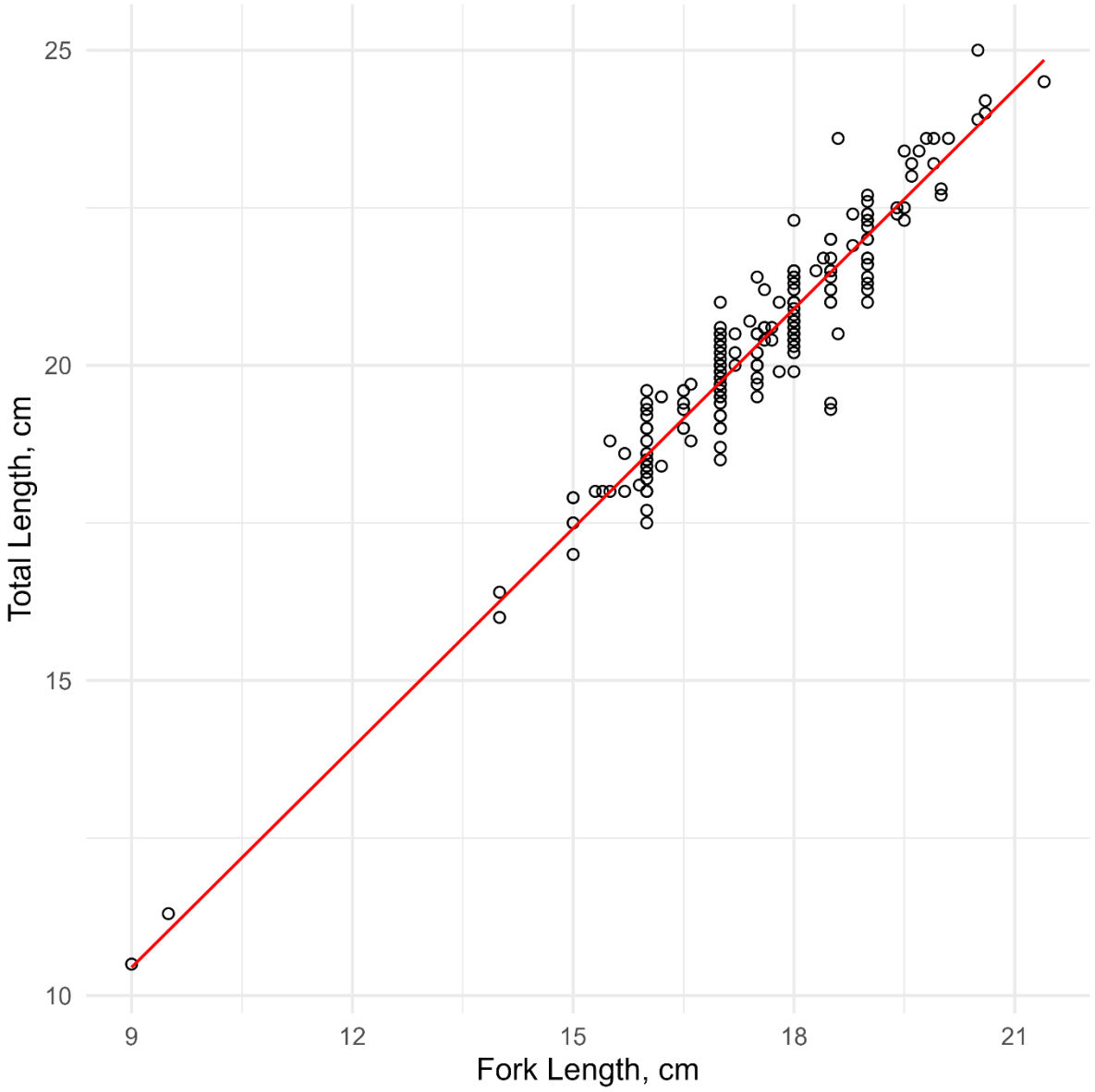

686

687 **Figure S3.3.** Allometry model predicting total length (TL) from fork length (FL) for 238
688 *Ctenochaetus striatus* individuals. The fitted model is TL = 1.161*FL.

689 The model S3.4, which is presented in Figures S3.1 and S3.1:

690 $$L = \beta_0 + \beta_1 \ln(A) \qquad S3.4$$

691 estimates body length (TL; cm), as a function of age (A; years). β_0 and β_1 are the parameters
692 to be estimated (fitted estimates in Table S3.1).

693 **Table S3.1.** Summary statistics for the fitted parameters the model (Equation S3.4).

Parameter	Estimate	Std. Error	t-value	p-value
β_0	14.58	0.133	109.57	<0.001

β_1	2.72	0.066	41.34	<0.001

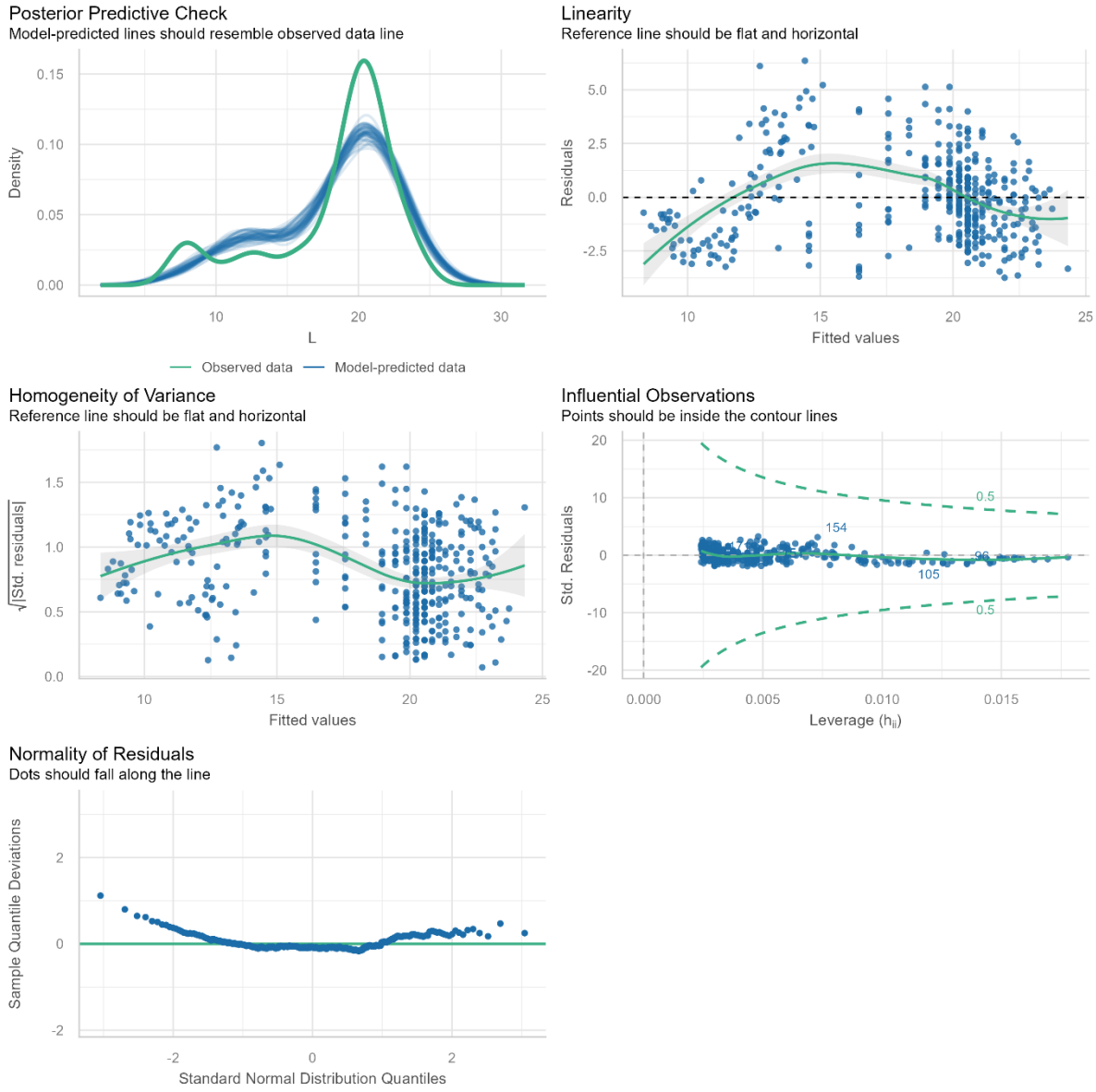

Figure S3.5. Otolith growth model (Equation S3.4) assumption checks performed by the *check_model()* function from the *performance* package (Lüdecke et al., 2021).

S4. Sensitivity analysis of the slope of the Lorenzen mortality

Changing the exponent (i.e., the slope on the log-log scale) of Lorenzen's mortality (a in the equation $\mu_i = 16.3{L_i}^a$), had little impact on the shape of the calculated growth-at-size (Figure S4.1A).

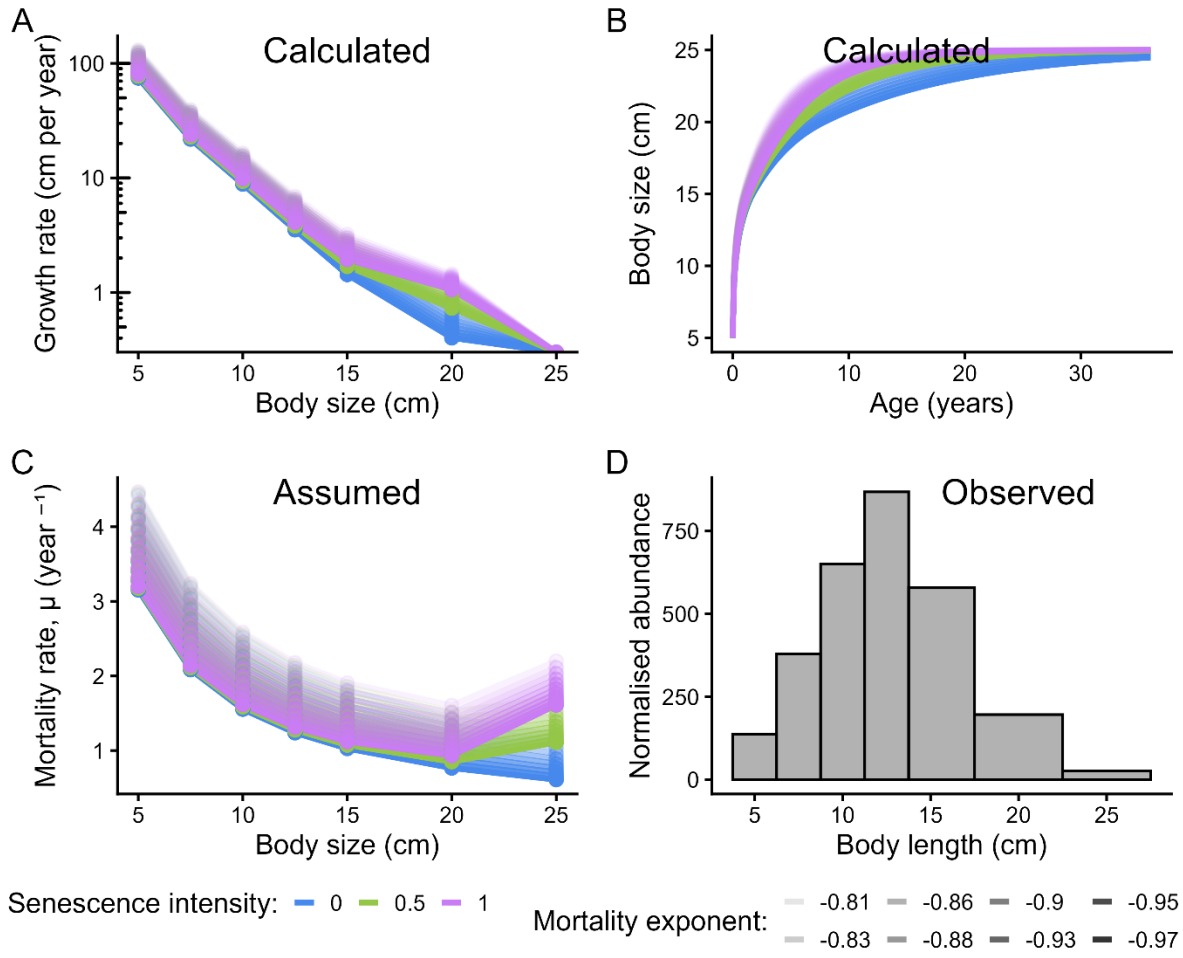

Figure S4.1. Estimated growth-at-size (A) and size-at-age (B) for 30 mortality scenarios, with 10 levels of Lorenzen mortality slope crossed with three levels of senescence mortality (C) that would result in the observed (D) length distribution of *Ctenochaetus striatus*.

References used in the Supplementary Material

Lüdecke, D., Ben-Shachar, M.S., Patil, I., Waggoner, P., Makowski, D., 2021. performance: An R Package for Assessment, Comparison and Testing of Statistical Models. Journal of Open Source Software 6, 3139. https://doi.org/10.21105/joss.03139

Trip, E.D.L., Craig, P., Green, A., Choat, J.H., 2014. Recruitment dynamics and first year growth of the coral reef surgeonfish Ctenochaetus striatus, with implications for acanthurid growth models. Coral Reefs 33, 879–889. https://doi.org/10.1007/s00338-014-1182-x